Morphological impact of low-energy Xe^+ irradiation on polycrystalline titanium targets

Morphological impact of low-energy Xe^+ irradiation on polycrystalline titanium targets

M A Garcia[1,2], R Gago[1], D Esteban-Mendoza[1], R Cuerno[3] and J Rickards[2]

[1]Instituto de Ciencia de Materiales de Madrid, Consejo Superior de Investigaciones Científicas, Cantoblanco 28049 Madrid, Spain
[2]Instituto de Física, Universidad Nacional Autónoma de México
Apartado Postal 20-364, Ciudad de México, Mexico
[3]Departamento de Matemáticas y Grupo Interdisciplinar de Sistemas Complejos, Universidad Carlos III de Madrid
Avenida de la Universidad 30 28911 Leganés, Spain

magarcia@ciencias.unam.mx

Abstract Low energy (1-keV) Xe^+ irradiation at different incidence angles (α) has been performed on pure polycrystalline Ti pellets at room temperature. The ion current was set between 110 and 200 μA cm^{-2} (ion flux ~ 7-12 $\times 10^{14}$ ions cm^{-2} s^{-1}). Changes of the surface morphology were characterized *ex-situ* with scanning electron microscopy and atomic force microscopy. Ion bombardment induces a significant surface roughening, with a complex morphology due to the polycrystalline nature of the targets. For $\alpha \leq 60^o$, ripple nanostructures appear within a long-range roughening. The ripple domains present a short-range order, with no orientation coherence between different domains or with respect to the ion beam. For $\alpha = 70^o$, large pillar-like structures appear aligned with respect to the ion beam. Finally, at gracing incidence ($\alpha = 80^o$), a smooth surface emerges with shallow ripples oriented parallel to the ion beam. The observed features can be interpreted as the result from the interplay between transport and erosion mechanisms, which are modulated by the initial material microstructure (grain and crystal size). Finally, the surfaces become more hydrophobic after ion irradiation, which can be exploited for biomedical applications.

1. Introduction

The surface modification of solid targets by ion beams is a well-known technique, used as an intermediate step in the fabrication of integrated circuits and related technologies [1,2]. The implantation of foreign atoms into the matrix of a target material induces changes of its electrical, optical and thermal properties [3]. Additionally, changes of the surface topography driven by ion irradiation is also a relevant matter of research, enabling even the production of self-organized nanostructures [1,2].

Tailoring the surface morphology of titanium (Ti) based targets is of great interest for biomedical applications [4], including both dental and orthopedic implants [5,6,7]. The emergence of surface features could contribute to an enhancement on the adherence and the proliferation of biomolecules onto the metal implant [8,9,10]. Both nanometer and micrometer features remain important scales for osteointegration, the former playing a greater role for biochemical processes in the beginning of the bone and metal implant interaction [6]. In this context, surface roughening by noble ion irradiation at low energies (up to few keV) is a promising technique that does not alter the chemical nature of the surface (in particular, retaining its biocompatibility). For example, Riedel and collaborators [5] have explored the growth, mobility and re-organization of mesenchymal stem cells (MSCs) osteoblast rat cells over Ti-6Al-4V alloys. It is found that there is a higher response for surfaces that have been treated with ion irradiation in comparison to those left untreated.

On the other side, a physical understanding of the processes that a surface undergoes during ion irradiation is of interest for controlling specific structures. Ion-induced surface features are known to depend on many experimental parameters including ion type, energy, angle of incidence, temperature, and target material [2]. At the current state of art, experimental knowledge ranges from insulating, semiconducting to metallic targets. Continuum theories based on ion-solid interactions within mesoscopic length scales have been applied successfully predicting the variability of the observed ion-induced patterns at surfaces. Particularly, theories based on the dependence of the sputtering yield on the local surface curvature as highlighted in the Bradley-Harper model [11] and subsequent extensions [12,13], as well as other hydrodynamic descriptions [2,14,15,16], have been able to predict many of the features that have been observed experimentally. However, in the case of metallic targets, which retain their crystalline character upon ion bombardment [3,15], other effects play important roles in addition to those observed in amorphous or amorphizable targets. Studies on metallic surfaces have derived in the identification of two main roughening regimes depending on the relevance of diffusive or erosive mechanisms [1,17,18]. In the first case, surface features emerge as a result of preferential crystallographic diffusion pathways due to Ehrlich-Schwoebel energy barriers [1,3]. For the second, surface features are defined by the ion beam direction on the surface. A great deal of advances has been achieved so far, and further progress can still be realized for appropriate applications.

2. Experimental techniques

Figure 1(a) shows a photograph to illustrate the type of targets used in this work. Commercially pure (99.6+%) Ti rods (grade 2) with 1-cm in diameter were purchased from Goodfellow Inc. [19]. 3-mm thick disks were obtained from cut-outs and mechanically polished by consecutive use of SiC sandpaper from 320 up to 4000 grit. Mirror-finished surfaces were obtained through 3-μm, 1-μm and ½-μm particle-sized diamond paste with micro-cloth on a polishing lap machine. Lastly, samples were cleaned with ethanol in an ultrasonic bath for 10 minutes to remove any left residues. Figure 1(b) shows the surface finished obtained with this method as assessed by scanning electron microscopy (SEM). The surface is rather flat and featureless except from the present of some scratches and some unavoidable remaining material from the polishing method.

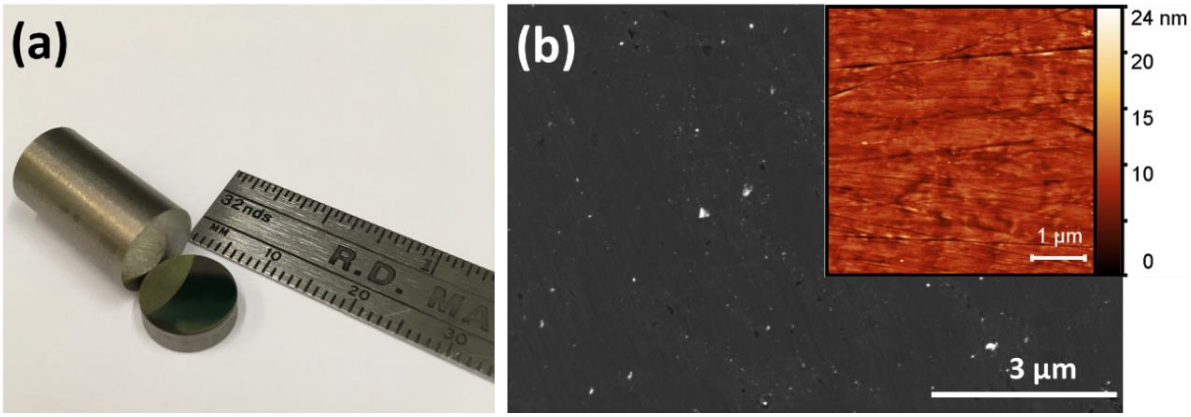

Figure 1. (a) Photograph of the targets used in this work: 3-mm height disks from 1-cm diameter titanium bars were cut and mechanically polished. (b) SEM image of the initial surface morphology of *as-polished* titanium samples before ion irradiation and AFM micrograph (inset). In this way, *as-polished* samples can be produced with a surface roughness below ~ 2 nm.

The ion irradiation has been performed with a 3 cm Kaufman-type ion gun. For this work, Ti targets have been irradiated with 1-keV Xe ions at different angles of incidence (α) ranging from normal to glancing geometries. The irradiations were performed at room temperature, meaning that no intentional heating was applied to the targets. The ion current has been varied between 110 to 200 μA cm^{-2} (ion flux of ~ 7 to 12×10^{14} ions cm^{-2} s^{-1}). The ion dose for all experiments exceeded 10^{18} ions cm^{-2}. After

irradiation, the surface morphology of the samples was characterized with SEM (FEI Verios 460, Instituto de Micro y Nanotecnología-CNM, CSIC), and atomic force microscopy (AFM; Agilent PicoPlus 5500, Instituto de Ciencia de Materiales de Madrid, CSIC). Data processing of the AFM topography was carried out using the Gwyddion free SPM data analysis software [20] for at least three different spots on the surface samples. Surface wettability measurements were obtained using ultra-pure (Milli-Q) water with a static contact angle instrument (CAM 101, KSV Instrument Ldt.). The result was averaged over at least four measurements at different locations per sample.

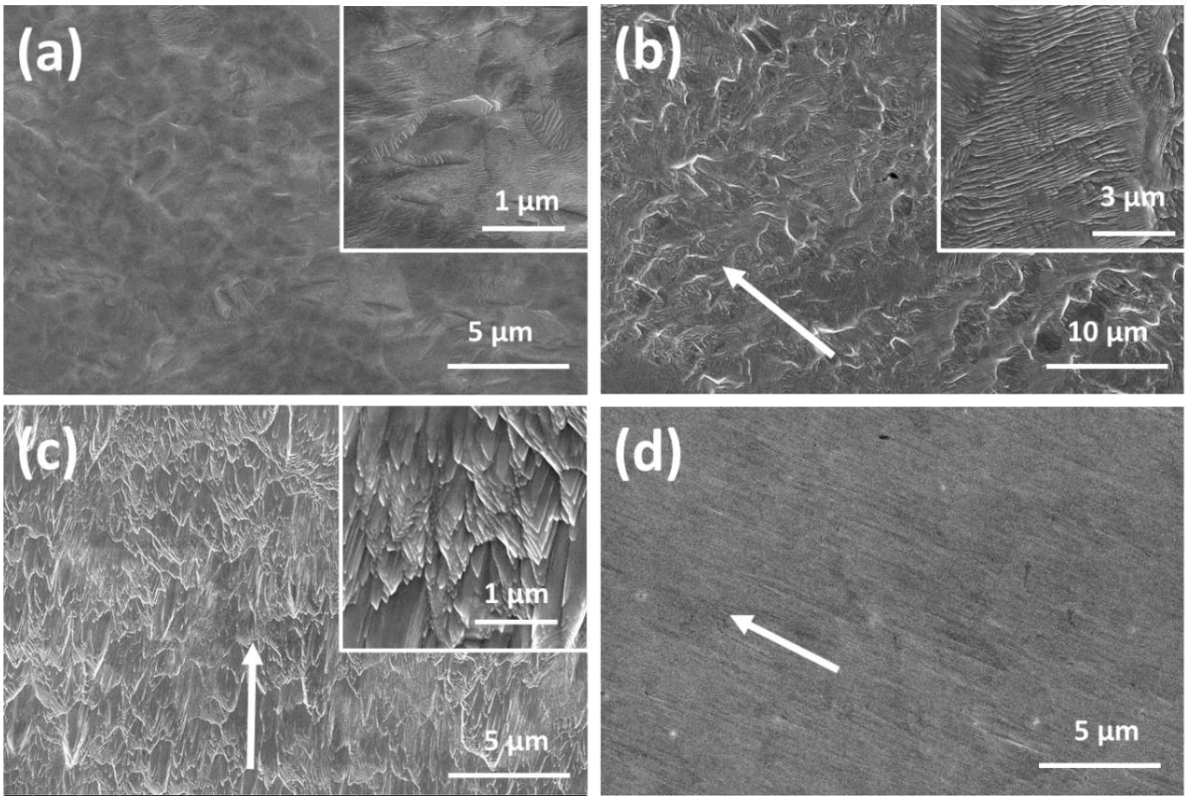

Figure 2. SEM micrographs of titanium irradiated surfaces at α = (a) 0°, (b) 60°, (c) 70° and (d) 80°. When shown, the arrow indicates the projected ion beam direction onto the surface. The insets are images of the surface features with a higher magnification.

3. Results and discussion

3.1 Scanning electron microscopy (SEM)

The surface morphologies of Ti surfaces after Xe^+ irradiation at different α obtained through SEM are shown in Figure 2. The arrows indicate the ion beam projection on the surface in the case of oblique irradiations. In comparison to the initial state of the surface (see Figure 1(b)), the ion irradiation induces pronounced morphological changes, which vary with the angle of incidence. In particular, for normal incidence irradiation (Figure 2(a)), a micrometer scale surface roughness develops with an underneath ripple nanostructure (with a 28-nm wavelength). The ripple structures are confined to domains of several microns in width, but there is no coherence on the orientation between the different domains. The overall surface morphology at 60° (Figure 2(b)) resembles that observed at 0º, although the features (both characteristic length and domain size) are considerably enlarged (note the scale bar). Here, ripple structures are also present and, even at off-normal irradiation, the ion beam does not imprint any preferred orientation. At some locations, the morphology displays also a faceted morphology. Further increase of the angle of incidence up to 70° (Figure 2(c)) leads to micron-size pillars and a clear

enhancement of the faceted terraces. The pillars are clearly oriented with respect to the ion beam, as an indication of ion sculpting effects. Finally, at glancing angles of incidence of $\alpha \approx 80°$ (Figure 2(d)), the surface is rather flat. In this case, shallow ripples appear with an orientation parallel to the ion beam.

The observed morphologies may be explained in terms of the competing mechanisms between transport and erosive effects of the bombarding ion into the target material. For example, the presence of ripples at normal incidence or the absence of preferred orientation, both support the role of diffusive-like instabilities. On the contrary, the relevance of erosive processes at high angles ($\geq 70º$) can be hinted by the appearance of oriented and faceted structures, see Sec. 3.2 below. Furthermore, the complexity and lack of long-range coherence of the surface morphology can be attributed to the polycrystalline nature of the targets [21,22]. In addition, the initial local inhomogeneous morphology resulting from the polishing process may also contribute to this dispersion. It should be noted that typical crystalline grains in commercially pure Ti range within a few micrometers in size [23]. Nonetheless, the results clearly show that ion irradiation at different angles can be used to tailor the surface morphology of the Ti targets.

3.2 Atomic force microscopy (AFM)

AFM analysis has been carried out to study the nanotopography with a greater detail and obtain quantitative information on surface features. Table 1 gives values for the maximum height (h_{max}) and root mean square (RMS) roughness (R_q) of the initial morphology and after irradiation at three incidence angles. In the case of h_{max}, it increases with respect to the pristine surface for α of 0º and 60º. However, similar values as in the initial state are retained at grazing angles ($\alpha = 80º$). The same trend is observed for the R_q values, with a roughness increase of one order of magnitude after irradiation at α up to 60º. The surface is still rougher with respect to the pristine case at $\alpha = 80º$. It should be noted that due to the local character of AFM and the limitation in the scan size by the relatively high ion-induced roughening, the values of R_q may be underestimated.

Table 1. Maximum height (h_{max}) and RMS roughness (R_q) for titanium surfaces at different angles of incidence (α). The values are obtained from the analysis of 4×4 μm^2 AFM images.

	As-polished	**α = 0°**	**α = 60°**	**α = 80°**
h_{max} (nm)	21 ± 4	130 ± 9	179 ± 30	25 ± 2
R_q (nm)	1.5 ± 0.2	15 ± 2	22 ± 4	3.1 ± 0.4

AFM can also be used to compare the ripple nanostructures produced at normal or 80° grazing incidence angle. As already pointed out, the origin of these ripples may be attributed to diffusion and erosion mechanisms, respectively. A detailed view of both type of ripples is shown in Figure 3 accompanied by one-dimensional profiles at the bottom. Remarkably, such nanostructures present a high degree of local order or coherence within a few hundreds of nanometers, which is a common feature of polycrystalline surfaces [18,21,22]. The characteristic wavelength of both type of ripples also differs significantly. In Figure 3(a), the ripples have a wavelength of a few tens of nm. On the contrary, the ripples in Figure 3(b) have a wavelength one order of magnitude larger. However, one significant difference is the degree of order. For normal incidence, the ripples are long and display a well-defined pattern. However, ripples obtained at grazing angle are rather short in length and highly disordered in vertical and horizontal directions.

For comparison, Riedel *et al*. [5] obtained surface ripples with 20 nm wavelength over Ti-Al-V surfaces bombarded with 1.1keV Ar^+ at normal incidence. Meanwhile, Toma *et al.* [24] obtained ripples of a few hundred nm on Ag thin films bombarded with 800 eV Ar^+ at 80° angle. As mentioned in the paper by Toma *et al*. [24], the range of attainable wavelengths is affected by the initial target out-of-plane grain size through shadowing effects. Nonetheless, for larger grains, surface ripples can propagate

into neighboring grains with slight mismatch. In any case, the reported wavelengths agree with our observations, suggesting similar underlying mechanisms on polycrystalline metal targets.

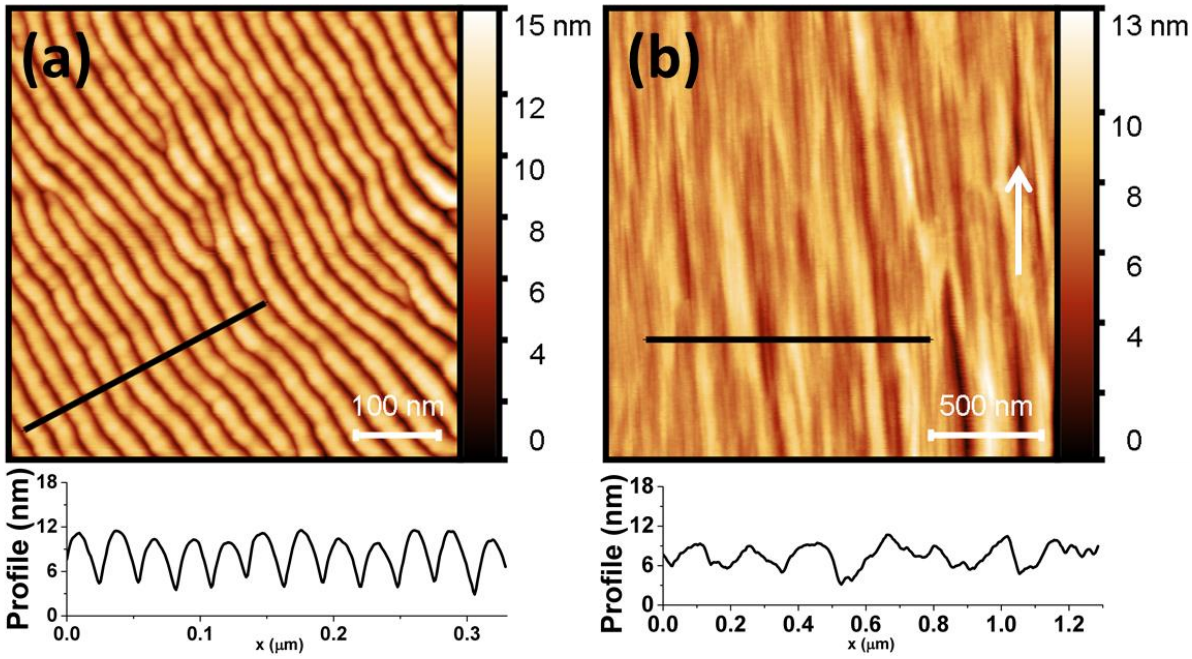

Figure 3. AFM micrographs of Ti targets after Xe^+ irradiation at α = (a) 0º (λ = 28 nm, R_q = 2.25nm) and (b) 80° (λ = 180 nm, R_q = 1.43 nm). For α = 80°, the arrow indicates the ion beam projection on the surface. One-dimensional profiles are given underneath the topography images.

3.3 Surface wettability

Wettability is a relevant factor for biomedical materials. There have been discussions about wettability of Ti surfaces regarding a possible direct link of water-based or protein-based molecules adsorption and its rate of osseointegration on the surface [7]. Surface roughness can affect the surface energy and, hence, change the wettability properties [25, 26]. Therefore, as a preliminary step to test the eventual application of ion-irradiated Ti as biomedical surfaces, static contact angle measurements were performed on control and irradiated samples. In any case, a deeper biomedical study of these surfaces is under way and will be presented elsewhere. As a summary, the interface static contact angle between the titanium surface and a droplet of water is given in Table 2. In the case of irradiated samples, the contact angle typically increases and, hence, present a more hydrophobic character with respect to *as-polished* surfaces. Therefore, ion irradiation may be used to tailor the biomedical response of Ti-based surfaces.

Table 2. Contact angle measurements of Ti surfaces after Xe^+ irradiation at different angles (α)

	As-polished	**α = 0°**	**α = 60°**	**α = 70°**	**α = 80°**
Contact angle (°)	79 ± 6	90 ± 3	90 ± 5	81 3	93 4

4. Conclusion

Low-energy noble ion irradiation of titanium substrates for surface topography modification has been performed at different angles of incidence. Surface characterization was carried out using surface analytical techniques including SEM and AFM. A significant roughening of the surface has been achieved, with a complex morphology related to the polycrystalline nature of the targets. In any case, the resulting morphologies can be related to instabilities due to diffusive or erosive processes. Ion irradiation has also an impact on the surface wettability, which becomes more hydrophobic. This result

and the conjunction of nanometer and micrometer-sized structures points out the potential implications into surface bioactivity. A deeper study of the biomedical performance of these surfaces is under evaluation and will be presented elsewhere.

Acknowledgments
We acknowledge Prof. L. Vázquez for fruitful discussions and support on AFM and Dr. Miguel Manso for support on contact angle measurements. We acknowledge the service from the MiNa Laboratory at IMN, and funding from CM (project S2018/NMT-4291 TEC2SPACE), MINECO (grants CSIC13-4E-1794, FIS2015-66020-C2-1-P, and PGC2018-094763-B-I00) and EU (FEDER, FSE). Additional financial support has been obtained from UNAM - PAPIIT IN-111717 (Mexico) and CONACyT (Mexico) Posdoctoral Fellowship.

References
[1] Chan W L and Chason E 2007 *J. Appl. Phys.* **101** 121301-46
[2] Muñoz-García J, Vázquez L, Castro M, Gago R, Redondo-Cubero A, Moreno-Barrado A and Cuerno R 2014 *Mater. Sci. Eng.* R **86** 1-44
[3] Buatier de Mongeot F and Valbusa U 2009 *J. Phys.: Condens. Matter* **21** 224022
[4] Rack H J and Qazi J I 2006 *Mater. Sci. Eng.* C **26** 1269-77
[5] Riedel N A, Williams J D and Popat K C 2011 *J. Mater. Sci.* **46** 6087-95
[6] Grandfield K 2015 *Phys. Today* **68** 40-45
[7] Le Guéhennec L, Soueidan A, Layrolle P and Amouriq Y 2007 *Dent. Mater.* **23** 844-54
[8] Grandfield K, Gustafsson S and Palmquist A 2013 *Nanoscale* **5** 4302-08
[9] Davies J E, Mendes V C, Ko J C H and Ajami E 2014 *Biomaterials* **35** 25-35
[10] Cai K, Bossert J and Jandt K D 2006 *Colloid Surf. B: Biointerfaces* **49** 136-44
[11] Bradley R M and Harper J M E 1988 *J. Vac. Sci. Technol.* A **6** 2390-95
[12] Cuerno R and Barabási A-L 1995 *Phys. Rev. Lett*. **74** 4746-49
[13] Makeev M A, Cuerno R and Barabási A-L 2002 *Nucl. Instrum. Methods Phys. Res.* B **197** 185-227
[14] Muñoz-García J, Cuerno R and Castro M 2008 *Phys. Rev.* B **78** 205408
[15] Bradley R M and Shipman P D 2010 *Phys. Rev. Lett.* **105** 145501
[16] Castro M, Gago R, Vázquez L, Muñoz-García J and Cuerno R 2012 *Phys. Rev.* B **86** 214107
[17] Valbusa U, Boragno C and Buatier de Mongeot F 2002 *J. Phys.: Condens. Matter* **14** 8153-75
[18] Ghose D 2009 *J. Phys.: Condens. Matter.* **21** 224001
[19] Goodfellow Inc. Corp. is based on Pennsylvania, USA.
[20] Nečas D and Klapetek P 2012 *Cent. Eur. J. Phys.* **10** 181-8
[21] Toma A, Chiappe D, Šetina Batič B, Godec M, Jenko M and Buatier de Mongeot F 2008 *Phys. Rev.* B **78** 153406-4
[22] Škereň T, Temst K, Vandervorst W and Vantomme A 2013 *New J. Phys.* **15** 093047
[23] Contieri R J, Zanotello M and Caram R 2010 *Mater. Sci. Eng.* A **527** 3994-4000
[24] Toma A, Šetina Batič B, Chiappe D, Boragno C, Valbusa U, Godec M, Jenko M and Buatier de Mongeot F 2008 *J. Appl. Phys*. **104** 104313-7
[25] Xu L-C and Siedlecki C A 2007 *Biomaterials* **28** 3273-83
[26] Bonn D, Eggers J, Indekeu J, Meunier J and Rolley E 2009 *Rev. Mod. Phys.* **81** 739-805